DAMPING OF HIGHLY EXCITED VIBRATIONS IN HEAVY NUCLEI

J. Wambach, B. Schwesinger

JOURNAL DE PHYSIQUE
Colloque C4, supplément au n°3, Tome 45, mars 1984 page C4-281

DAMPING OF HIGHLY EXCITED VIBRATIONS IN HEAVY NUCLEI

J. Wambach† and B. Schwesinger*†

†*Institut für Kernphysik, Kernforschungsanlage Jülich, D-5170 Jülich, F.R.G.*
**Department of Physics, State University of New York at Stony Brook, Stony Brook, NY 11794, U.S.A.*

Résumé - Nous présentons un modèle décrivant l'atténuation de l'intensité des transitions 1 particule-1 trou dans des excitations plus complexes. Les canaux 2 particules-2 trous sont traités explicitement tandis que les configurations d'ordre plus grand le sont approximativement. Nous employons pour la fonction de réponse linéaire une expression équivalent à la diagonalisation de l'interaction résiduelle dans les sous-espaces 1p-1t et 2p-2t combinés. Les implications pour les excitations de parité naturelle et non naturelle dans ^{90}Zr et ^{208}Pb sont discutées.

Abstract - We present a model which describes damping of 1p-1h transition strength into more complicated nuclear excitations. 2p-2h decay channels are treated explicitly and higher configurations in an approximate way. We use an expression for the linear response function which is equivalent to a diagonalization of the residual interaction in the combined 1p-1h and 2p-2h subspaces. Implications for natural and unnatural parity excitations in ^{90}Zr and ^{208}Pb are discussed.

I - INTRODUCTION

The microscopic understanding of damping of nuclear collective motion has attracted theoretical interest in the last few years. Considerable progress has been made especially for simple nuclear excitations like single-particle and vibrational states (see ref. 1 for a recent review).

Generally two damping mechanisms can be identified for vibrations:

(i) pure mean field damping which gives rise to a spreading of 1p-1h strength due to shell structure ("fragmentation width") and a broadening above the continuum threshold due to particle emission ("escape width").

(ii) damping from residual two-body collisions, which couple the 1p-1h doorway states to nuclear compound states ("spreading width").

With increasing mass number mean field effects become less important /2/, at least for low energy resonances, and the decay largely proceeds via more complicated states. Their level density increases rapidly with excitation energy and microscopic descriptions of damping become difficult because of the enormous number of states to be taken into account.

We present a model which treats 1p-1h and 2p-2h states explicitly and higher compound states in an approximate way. In the restricted space of 1p-1h and 2p-2h excitations a diagonalization iterates the p-h irreducible diagrams of order V^2 to all

orders. This procedure is equivalent to a diagonalization of V in the full subspace /3/. Since all 2p-2h configurations in a model space of two major shells above and below the Fermi surface are retained the model is especially powerful for describing the high energy dispersion of strength.

In section II we give a brief outline of the theory and section III presents results for ^{90}Zr and ^{208}Pb. First, natural parity excitations are discussed. We also present the isobaric analog state (IAS) which is an approximate eigenstate of the nuclear hamiltonian. This constitutes a stringent test for models of strength dispersion. Furthermore isospin interference effects enhanced by 2p-2h coupling are considered for the quadrupole response in ^{208}Pb. In the sector of unnatural parity excitations we show results for "the twist mode", a mode propagating via transverse zero sound. The high energy dispersion of Gamow-Teller strength in ^{90}Zr and ^{208}Pb is also discussed.

II - OUTLINE OF THE MODEL

The distribution of nuclear transition strength S to a weak external perturbation

$$\hat{Q}(t) = 1/2\ (Q\ e^{-i\omega t} + Q^{+}\ e^{i\omega t}) \tag{2.1}$$

is given by the linear response function

$$S_Q(\omega) = -\frac{Im}{\pi}\left\{\langle|\, Q^{+}(\omega-H+E_0+i\eta)^{-1} Q\,|\rangle - \frac{|\langle|\, Q\,|\rangle|^2}{\omega+i\eta}\right\} \tag{2.2a}$$

$$= -\frac{Im}{\pi} \sum_{\substack{npnh \\ n'ph'h}} \langle|\, Q^{+}\,|(npnh)\rangle\langle(n'pn'h)|\, Q\,|\rangle\, C_{nn'}(\omega+i\eta)^{-1}$$

with

$$C_{nn'}(\omega+i\eta) = \langle(npnh)|\omega-H+E_0+i\eta|(n'pn'h)\rangle \tag{2.2b}$$

Here H is the full nuclear hamiltonian, $|\rangle$ the exact ground state with energy E_0 and η an infinitesimal positive quantity. The calculation of S_Q involves inversion of the complex matrix $C_{nn'}$, which is of course impossible due to the huge number of states involved. Empirically, however, the strength function exhibits gross structures due to the fact that Q is a one body operator and the main contribution to S_Q comes from n=n'=1. Therefore to a very good approximation we only need the inverse of $C_{nn'}$ in the space of 1p-1h excitations. In terms of a projector P onto this space

$$P = \sum |1p1h\rangle\langle 1p1h| \tag{2.3}$$

we obtain

$$S_Q(\omega) = -\frac{Im}{\pi}\langle|\, Q^{+}P\{\omega-H_0-V+E_0+i\eta+V(1-P)(\omega-H_0-V+E_0+i\eta)^{-1}(1-P)V\}^{-1}PQ\,|\rangle \tag{2.4}$$

The operator 1-P projects onto the space complementary to 1p-1h, i.e. contains 2p-2h and higher excitations. In the specific calculation presented below the 1p-1h model space is spanned by 2 major shells above and below the Fermi surface (with discretized continuum states). The hamiltonian H has been split into a mean field part H_0 and a residual interaction V. V can only couple np-nh states with n<2 to the 1p-1h doorway, i.e. the entrance channel for the decay is given by the 2p-2h states only. We truncate 1-P at this level

$$1\text{-}P \sim \sum |2p2h\rangle\langle 2p2h| \qquad (2.5)$$

and treat the more complicated states n=n'>2 on the average by introducing a finite imaginary part $i\Delta$ in the 2p-2h propagator (Δ = 3 MeV is used). Furthermore V is neglected in the 2p-2h space which is a reasonable approximation at high frequencies since the level density $\rho_{2p2h}(\omega)$ is large and the detailed energy distribution unimportant. A finite $i\Delta$ in the 2p-2h propagator also compensates for the neglected residual interaction in the 2p-2h space which redistributes the strength coupling to the 1p-1h states. The interaction diagrams which are iterated by eq. (2.4) are given in Fig. 1. To order V^2 we have selfenergy insertions on the particle or hole line (which are diagonal in the 1p-1h indices) and ph-linked diagrams in which either a ph-pair (bubble diagram) or a pp- or hh-pair (ladder diagram) is exchanged between ph-states. Since the set of V^2 diagrams is complete one can show that $S_Q(\omega)$ is positive definite for all frequencies $\omega>0$.

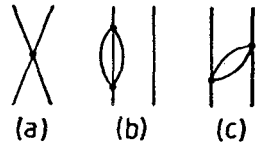

Fig. 1 - Interaction diagrams up to order V^2 iterated in S_Q (eq. (2.4)).

We have chosen a phenomenological nuclear hamiltonian

$$H_o = -\frac{\hbar^2}{2m^*}\Delta + U(\underset{\sim}{r}) \qquad (2.6)$$

where $U(\underset{\sim}{r})$ is a Woods-Saxon well. The nucleon effective mass m* is an adjustable parameter. V is approximated by an antisymmetrized zero range interaction

$$V(\underset{\sim}{r},\underset{\sim}{r}') = \{V_{00}[\rho] + V_{01}[\rho]\vec{\tau}\vec{\tau}'\}\,\frac{1}{2}\{1-P^{\sigma\tau}\}\delta(\underset{\sim}{r}-\underset{\sim}{r}') \qquad (2.7)$$

with linear density dependence

$$V_{\sigma\tau}[\rho] = V^{in}_{\sigma\tau}\rho(R) + V^{ex}_{\sigma\tau}(1-\rho(R)) \qquad (2.8)$$

$$\rho(R) = (1 + \exp(R-R_o)/\alpha)^{-1} \;;\; (\underset{\sim}{R} = (\underset{\sim}{r}+\underset{\sim}{r}')/2)\ . \qquad (2.9)$$

The parameters of V and m*/m used are listed in Table 1.

V^{in}_{00}	V^{ex}_{00}	V^{in}_{01}	V^{ex}_{01}	R_o	α	m*/m
107.3	-876.2	321.9	339.8	5.22 6.90	0.6	0.85

Table 1 - Strength of the residual interaction V as specified in eq. (2.7) in MeV fm^3. The two values for the interpolation radius R_o are in ^{90}Zr and ^{208}Pb respectively.

To discuss qualitative features of the response function S_Q it is useful to define operator averaged quantities like the average ph energy

$$\langle \varepsilon_{ph} \rangle_Q = \sum_{ph} Q^+_{ph} \varepsilon_{ph} Q_{ph} / \sum_{ph} Q^+_{ph} Q_{ph} \tag{2.10a}$$

the average interaction strength to first order

$$\langle V \rangle_Q = \sum_{\substack{ph \\ p'h'}} Q^+_{ph} V_{php'h'} Q_{p'h'} / \sum_{ph} Q^+_{ph} Q_{ph} \tag{2.10b}$$

and the frequency dependent second order term

$$\langle V(\omega)^2 \rangle_Q = \sum_{\substack{ph \\ p'h'}} Q^+_{ph} V_{ph;2p2h} (\omega - \varepsilon_{2p2h} + i\eta)^{-1} V_{2p2h;p'h'} Q_{p'h'} / \sum_{ph} Q^+_{ph} Q_{ph} \tag{2.10c}$$

Since for finite η $\langle V^2 \rangle$ is complex we obtain a frequency dependent energy shift

$$\Delta E_Q(\omega) = \mathrm{Re} \langle V(\omega)^2 \rangle_Q \tag{2.11a}$$

and a width

$$\Gamma_Q(\omega) = 2\mathrm{Im} \langle V(\omega)^2 \rangle_Q \tag{2.11b}$$

In terms of these quantities one can define an operator averaged response as

$$\langle S_Q(\omega) \rangle = \langle |Q^+ Q| \rangle P_Q(\omega) \ . \tag{2.12a}$$

Here

$$P_Q(\omega) = \frac{1}{2\pi} \frac{\Gamma_Q(\omega)}{(\omega - E^0_Q + \Delta E_Q(\omega))^2 + 1/4 \ \Gamma_Q(\omega)^2} \tag{2.12b}$$

is the probability for finding transition strength induced by Q at frequency ω. E^0_Q in the denominator denotes the unperturbed energy $\langle \varepsilon_{ph} \rangle_Q$ plus the first order correction $\langle V \rangle_Q$. Note that in the limit where the transition strength is concentrated in a single state $|n\rangle = Q|\rangle$ expression (2.12) becomes exact. Comparison of $\langle S_Q \rangle$ with the exact S_Q shows that the average gives a good representation of the gross features of the response like the centroid energy and the variance if the resonance is localized on the 1p-1h level.

III - RESULTS

Monopole vibrations

Monopole vibrations are compressional modes of the nucleus and hence give information on the bulk moduli in symmetric nuclear matter and (via N≠Z nuclei) also in asymmetric nuclear matter. The damping of the isoscalar and isovector branches is quite different as we shall discuss. Bertsch /5/ first pointed out that the width of the isoscalar monopole vibrations is very small because of a strong interference between ph-unlinked and ph-linked diagrams. In isospin symmetric nuclear matter the imaginary parts of selfenergy and bubble diagrams cancel to order q^2/k_F^2 for spin scalar isospin scalar density modes as discussed in ref. 6. This is also true to a very large extent for a finite nucleus /7/. Fig. 2 displays $\Gamma_Q(\omega)$ in the long wavelength limit for $Q = r^2$ and $Q = r^2 \tau_o$. In the isoscalar channel one observes remark

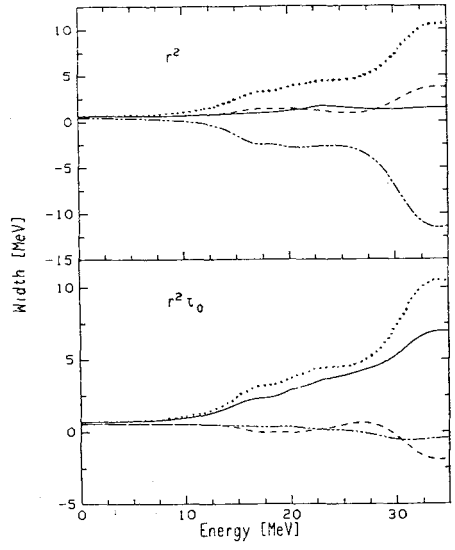

Fig. 2 - Operator averaged width for isoscalar (upper part) and isovector (lower part) monopole excitations in ^{208}Pb. The dotted line indicates contributions from selfenergy diagrams and the dashed and dash-double dotted lines give ladder and bubble terms. The full line represents the sum.

able cancellation of selfenergies and bubbles (dash-dotted and dash-double dotted lines). The ladders (dashed lines) only play a minor role. The situation in the isovector channel is quite different. Bubble contributions are substantially reduced and ladders instead of enhancing reduce the width somewhat at higher frequencies. These average features are also present in the full calculation (Fig. 3).

The isoscalar transition strength (upper part) remains fairly localized after 2p-2h mixing is turned on and the increase in "width" has to be interpreted as a redistribution of strength between nearby 1p-1h doorway states (dotted lines) via 2p-2h interactions. Note that the centroid is shifted due to a repulsive contribution from bubbles to $\Delta E_0(\omega)$ which is well known in symmetric nuclear matter /8/. The second order shifts are quite sizable. While $\langle V \rangle_0$ is about -4 MeV in ^{90}Zr and -3.3 MeV in ^{208}Pb at the resonance energy the shift from bubbles is 2 MeV in both nuclei. For isovector modes the situation is different. Particle and hole spreading dominate the decay and hence Γ_0 is large. Consequently the modes are strongly damped (middle part of Fig. 3).

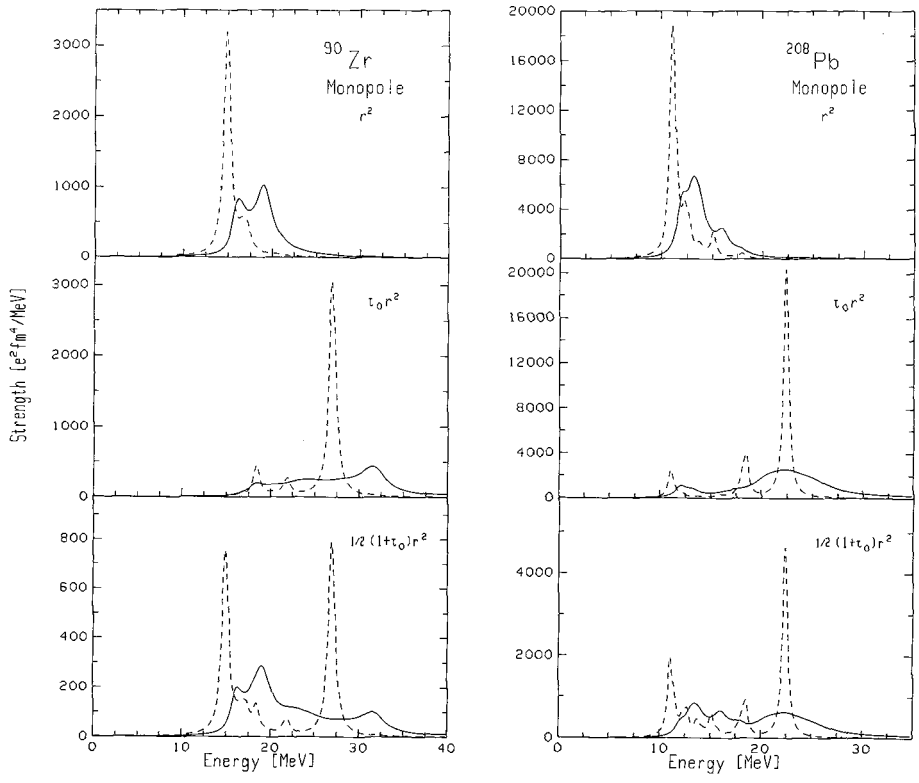

Fig. 3 - Monopole response in ^{90}Zr (left part) and ^{208}Pb (right part). The dashed lines give 1p-1h alone while the full line includes 2p-2h.

Quadrupole modes

In the quadrupole response we see the same features: little damping of the isoscalar vibration (upper part of Fig. 4) due to large cancellation of selfenergies by bubbles and a large spreading of isovector strength (middle part of Fig. 4). Note the very long high energy tail which in ^{90}Zr extends up to 50 MeV and in ^{208}Pb up to 40 MeV. The isovector FWHM in ^{90}Zr has been reported by Pitthan /9/ as 7-8 MeV. We find roughly 11 MeV somewhat larger than experiment. There are, however, theoretical uncertainties in the interaction as well as experimental difficulties in the background subtraction for broad resonances.

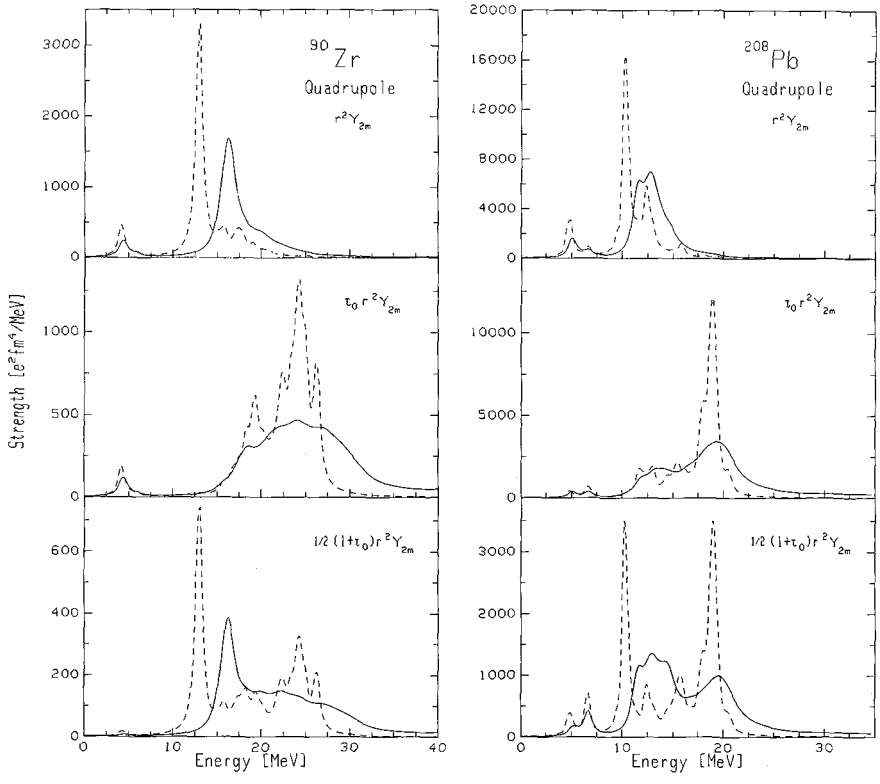

Fig. 4 - Quadrupole response in ^{90}Zr (left part) and ^{208}Pb (right part). The dashed lines give 1p-1h alone while the full line includes 2p-2h.

Charge exchange isovector monopole

Not only the giant dipole, also isovector monopole excitations provide information about the bulk and surface symmetry energies. The $r^2\tau_+$-resonance in the charge exchange channel is of special interest since its width is expected to be much narrower than the $r^2\tau_o$ - or the $r^2\tau_-$ -partners /10/. The latter is pushed up to higher energies by the Coulomb displacement energy E_C and the proton-neutron mass difference M_{pn} relative to $r^2\tau_o$. Monopole states in the (N+1,Z-1)-nucleus, however, are lowered by the same amount. The 2p-2h level density is much smaller reducing the phase space for the decay. The calculated strength distributions in ^{90}Zr and ^{208}Pb are shown in Fig. 5. The shape of the isovector monopole in ^{90}Y is similar to that in ^{90}Zr both on the 1p-1h level (dashed lines in Fig. 3 and Fig. 5) and on the 2p-2h level (full lines in Fig. 3 and Fig. 5). But there are distinct differences in ^{208}Tl and ^{208}Pb because of Pauli blocking effects. Due to the neutron excess the 3p and 2f neutron orbits are occupied and therefore the analogs of the strong 3p→4p and 2f→3f neutron transitions are missing (Fig. 5). Similarly the 2p→3p and 1f→2f transitions are blocked. The coupling to 2p-2h states affects the 1p-1h strength only slightly. The reason for this is the reduction of the level density from ~ 800/MeV in the parent nucleus to 200/MeV in the daughter nucleus. In ^{90}Y the calculated width is quite consistent with inelastic (π^-,π^o) scattering by Bowman et al. /11/ which gives roughly 14 MeV. In view of the fact, that in ^{208}Tl the escape width of the charge

exchange monopole may be small /12/ there is evidence from our calculation that the strength remains localized and can be seen in charge exchange reactions.

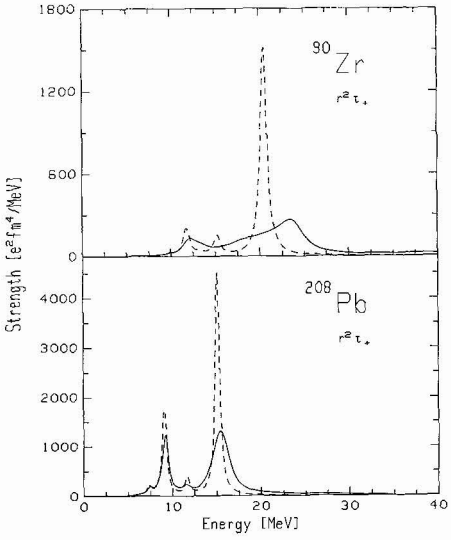

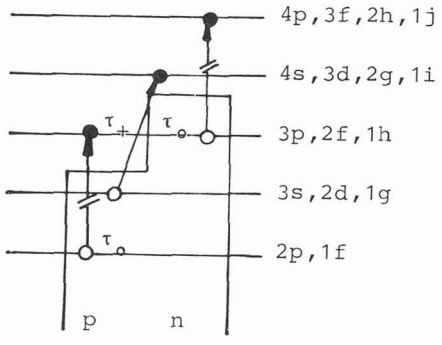

Fig. 5 - Isovector charge exchange monopole in ^{90}Zr and ^{208}Pb (left part). The effects of Pauli blocking in ^{208}Pb are displayed schematically in the right part.

The giant dipole resonance

The giant dipole is the experimentally best known giant resonance. It still has problems in the theoretical description. The value of the nuclear matter bulk symmetry energy ß between 28-36 MeV /13/ gives dipole excitation energies in nuclei which are too low. In Fermi liquid theory there is a simple relation between ß, the Landau parameter in the nuclear interior $f_0'^{(in)}$ and the quasiparticle effective mass

$$ß = 1/3\ k_F^2/2m^*\ (1 + 2f_0'^{(in)}) \ . \qquad (3.1)$$

With m*=m one obtains from ß = 28 MeV $f_0' = 0.53$. To fit the dipole energy systematics one needs $f_0' \tilde{=} 1$ for m*=m /14/. In our model the Landau parameter has to be obtained from order V and V^2. The ph-linked V^2 contributions to the energy are small however, such that the strength of the $\tau\tau'$-piece of V determines f_0'. We fixed f_0' from a bulk symmetry of 30 MeV from eq. (3.1). It has been suggested that the rapid "off the energy shell variation" of the effective mass might produce additional repulsion to the dipole energy. This effect is included in our model since the real part of the selfenergy diagrams which gives a ω-dependent correction to the single particle energies /15/, is retained. Fig. 6 displays the results of the calculation in ^{90}Zr and ^{208}Pb. We see almost no shift in the resonance position as 2p-2h states are coupled to the 1p-1h response. Decomposition into the various diagrams shows negligible contributions from the bubbles, a very weak repulsion from the ladders and a weak attraction from the selfenergies. The higher order corrections are too weak to place the dipole at the right position if only nuclear matter information is used. The solution might be provided by the surface dynamics in a nontrivial way: (i) our model neglects residual interaction in the 2p-2h space. Particle-hole rescattering terms (Fig. 7) will build up collective surface modes. Inclusion of those

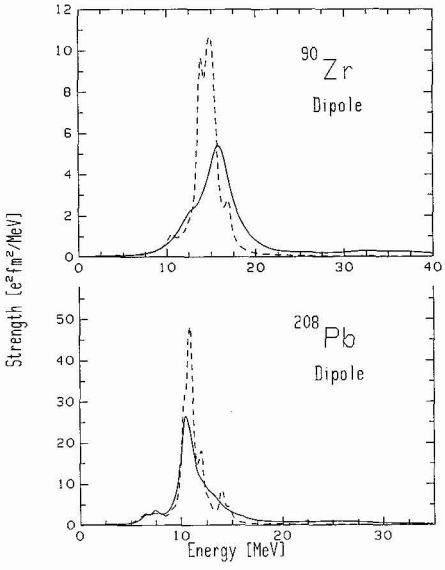

Fig. 6 - Giant dipole resonances in ^{90}Zr and ^{208}Pb. 1p-1h results are represented by the dashed lines, while the full lines include 2p-2h.

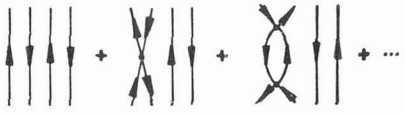

Fig. 7 - Rescattering diagrams in the 2p-2h space neglected in the present calculation.

rescattering terms /16/ changes the ω-dependence of the effective mass and therefore enhances off-shell effects. (ii) the density dependence of $V_{01}[\rho]$ is crucial for the ratio between surface and volume symmetry energy /17/. Our density dependence is rather weak (Table 1) giving a small surface symmetry energy.

The high energy dispersion of transition strength is not only a feature of the isovector monopole and quadrupole response functions, which are in an energy region of high level density, but is also seen in the dipole (full line in Fig. 6). The integrated strength in the tail ($\omega > 22.5$ MeV in ^{90}Zr and $\omega > 15$ MeV in ^{208}Pb) are 13 % and 10 % respectively. The classical Thomas-Reiche-Kuhn sum rule is exceeded by about 20 %. This corresponds roughly to the amount of energy weighted strength in the tail. Thus the energy weighted strength under the peak exhausts the sum rule.

Isobaric analog states and isospin mixing

If effects from the Coulomb interaction could be neglected the isobaric analogue state

$$|IAS\rangle = T_- |\rangle$$

would be an eigenstate of H, since then T_- commutes with the hamiltonian. This is the reason why, experimentally, the IAS is an extremely sharp resonance although it lies in a region with a high density of 2p-2h states.

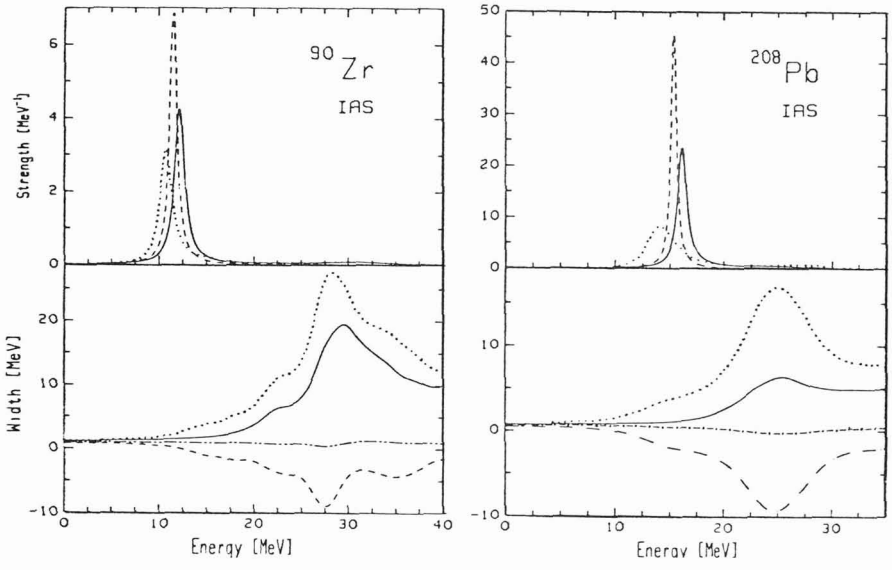

Fig. 8 - Isobaric analog strength distributions in ^{90}Zr and ^{208}Pb (upper part). The dashed lines give 1p-1h only. The dotted lines include 2p-2h mixing from selfenergy diagrams and the full lines include all diagrams. The lower part gives the various contributions to the widths. Ladders are indicated by the dashed lines, bubbles by the dash-double dotted lines and selfenergies by the dotted lines. The full lines give the sum.

We have looked at the width of this state in ^{90}Zr and ^{208}Pb as a check of our model. Fig. 8 shows the 1p-1h result which is given by the dashed line. The finite width here is a mathematical artifact coming from the finite imaginary $i\Delta$ introduced to allow numerical inversion of the strength function. The dotted lines show the effects of the selfenergy insertions which results in a broadening comparable to the single particle width. The inclusion of all second order terms cancels to a large extent the single particle width restoring partly isospin symmetry. The bottom of Fig. 8 indicates that this cancellation is due to the ladder diagrams and that the bubbles do not contribute. The cancellation between selfenergy and ladder, however, is not complete since for ^{90}Zr and ^{208}Pb 17 % of the strength resides in the high energy tail. Clearly, a better description would require consideration of ground state correlations /18/, because the ground state used must be an eigenstate of H if the symmetry argument is to hold.

Fig. 9 displays the response function to the electromagnetic quadrupole operator

$$Q_{2m} = \frac{1}{2} (1 + \tau_o) \, r^2 \, Y_{2m}$$

(full line) in comparison to the sum of isoscalar ($1/2 \, r^2 \, Y_{2m}$) and isovector ($1/2 \, \tau_o \, r^2 \, Y_{2m}$) response (dashed line). Since N≠Z for ^{208}Pb the two curves need not coincide and indeed we observe a rather large destructive interference. This is due to the fact that the coupling to 2p-2h configurations carries isovector strength

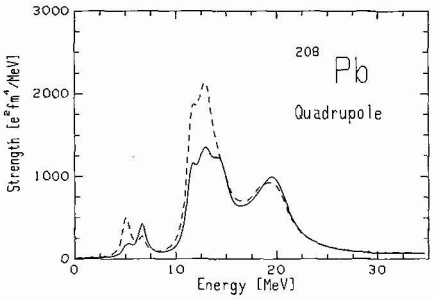

Fig. 9 - Isospin interference effects in the quadrupole response of ^{208}Pb. The sum of isoscalar ($1/2\ r^2Y_{2m}$) and isovector ($1/2\ \tau_0 r^2Y_{2m}$) strength indicated by the dashed line is compared to the electromagnetic ($1/2(1+\tau_0)r^2Y_{2m}$) response.

down to the region where isoscalar strength is concentrated (on the 1p-1h level the two peaks are well isolated). The destructive interference observed here moves 18 % of the strength out of the isoscalar peak and might provide the explanation to the observed differences in E2 strength from (e,e') and (α,α') /19/.

The twist mode

One of the more exotic nuclear resonances that has been speculated upon /4/ is the nuclear twist. Its motion can be visualized as a rotation of the different layers of a Fermi fluid against each other, the angle of rotation around the z-axis being proportional to the z-coordinate of the layer (Fig. 10).

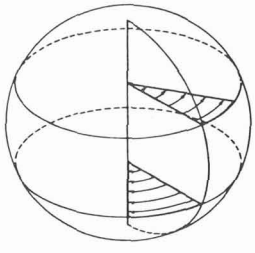

Fig. 10 - Velocity field for the lowest excited 2^- "twist mode".

In a fluid dynamical description the velocity field of the twist is purely rotational. Such a motion is only possible if there are tangential restoring forces effective in the fluid. The twist propagates via collisionless transverse zero sound so its energy is independent of F_0 (i.e. the nuclear incompressibility) and since it is a spinless mode, it is of course also independent of G_0:

$$E_{tw} = 2.3 \frac{k_F}{m^*} \sqrt{\frac{1}{5}(1 + \frac{1}{3}F_1)}R^{-1} \sim 45\ A^{-1/3}\ \text{MeV} \qquad (3.2)$$

For ^{208}Pb this gives an energy of $E_{tw} = 7.6$ MeV.

Microscopically the twist motion is expressed most easily through an operator of the form

$$T_{em} = \sqrt{\frac{5}{\pi}}\mu_N \sum_{i=1}^{A} \frac{1}{2}(1+\tau_i^0) z_i \ell_{z_i} = \sqrt{\frac{10}{3\pi}}\mu_N \sum_{i=1}^{A} \frac{1}{2}(1+\tau_i^0) \{\underset{\sim}{r}_i \times \underset{\sim}{\ell}_i\}_{J=2,M=0} \qquad (3.3)$$

acting on the corresponding ground state. The special combination of isospin operators chosen in (3.3) restricts the twist to protons only. In this case T_{em} is the orbital part of the electromagnetic M2 operator thus indicating a way to excite the mode. However, the M2 operator also contains a spin part

$$S_{em} = \sqrt{\frac{15}{2\pi}}\,\mu_N \sum_i \left(\frac{g_p+g_n}{2} + \tau_3 \frac{g_p-g_n}{2}\right) [\underset{\sim}{r}_i \times \underset{\sim}{\sigma}_i]_{J=2} \qquad (3.4)$$

which contributes 80 % to the M2 strength in ^{208}Pb leaving only 20 % for the twist. Therefore it seems very likely, that twist strength will be obscured by spinflip strength in (e,e') experiments /20/.

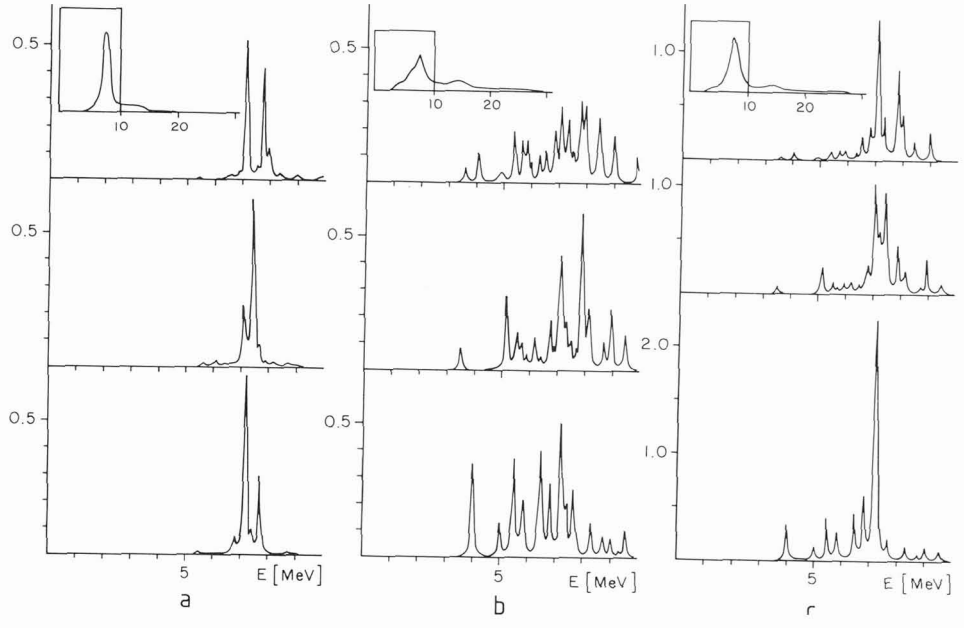

Fig. 11 - Low energy 2^- response: (a) denotes the twist part without interaction (lower part), V included to first order (middle part) and to second order (upper part), (b) displays the same for the spin part and (c) gives the total electromagnetic strength.

However, the situation turns out to be much more favourable as is demonstrated in Fig. 11. Each figure displays the response of ^{208}Pb to the operators indicated and contains three cases and one smaller inset. The bottom graph in each shows the strength function for the case of no residual interaction at all (V=0), i.e. the hamiltonian is just made from single particle energies. The middle section displays the case where the residual interaction between 1p-1h configurations only is taken into account whereas the upper curve gives the result of the full calculation coupling 2p-2h to the 1p-1h states. All three curves cover the energy range of 0-10 MeV. The inset in the top graph shows the result of the full calculation in the 1p-1h+2p-2h space over the energy range 0-30 MeV. All curves are normalized to the total electromagnetic strength in the range of 0-30 MeV

$$S_{M2} = 3.7\times10^4\ \mu_N^2 fm^2 .$$

The most striking feature exhibited by the results is the sharp concentration of the twist strength around 7 MeV. This concentration is already present in the single particle energies alone. Adding a residual interaction among the 1p-1h states has only little effect on the strength distribution, and actually a variation of the interaction parameters over a large range does not move the twist from its unperturbed position. Clearly this reflects the findings from fluid dynamical descriptions, that the energy of the twist does not depend on the Landau parameter F_0. Coupling the 2p-2h configurations to the 1p-1h states finally breaks the twist into two pieces, one at 7.2 MeV and one at 7.9 MeV.

In contrast to the twist, the fragmentation of spin flip strength is already present with no interaction at all and pertains when the interaction and 2p-2h couplings are added. The inset in Fig. 11b shows that 30 % of the spin flip strength resides above 10 MeV. 30 % however must be considered as a lower bound on the dispersion, for two reasons: (i) the effective G_0' resulting from the antisymmetrized zero range interaction used here is too small. Any finite range interaction, which we had to discard because of computational limitations, would shift the spin flip states to higher energies where the density of 2p-2h states is higher. This shift would result in an even stronger dispersion of the spin flip strength from the 2p-2h states. (ii) We have not introduced any mechanism to quench magnetic strength such as isobar-hole excitations. Such mechanisms only affect the spin flip modes and thus enhance the relative importance of the twist to the M2-sum.

Considering these two effects, it seems very likely that the 25 % M2 strength found experimentally /20/ in the energy range between 6-9 MeV is almost entirely due to the twist which contributes 20 % to the M2 sum. Fig. 4 shows that even with the rather large amount of spin flip strength located below 9 MeV the electromagnetic response is dominated by the twist peaks.

Let us examine the particle hole amplitudes of the twist operator. Because $z\ell_z$ is a spinless $1\hbar\omega$ operator connecting $\Delta L=1$ states only, the largest ph amplitudes are $(n,j,\ell+1)(n,j-1,\ell)^{-1}$ giving

$$\langle 0|z\ell_z|\{(n,\ell+1)\times(n,\ell)^{-1}\}_{2^-,0}\rangle = (-)^{\ell+1}\sqrt{\frac{\ell(\ell+1)(\ell+2)(2\ell+3)}{15}} . \qquad (3.5)$$

Therefore the twist is mainly built up from states where both particle and hole have high angular momenta. Table 2 shows some of the more important ph-states participating in the twist motion where energies of states designated by an asterisk have been measured experimentally.

p	h	(ph)-energy	rel. weight
$1i^*_{13/2}$	$1h^*_{11/2}$	7.2	.46
$1h^*_{9/2}$	$1g_{7/2}$	7.7	.31
$2f^*_{7/2}$	$2d^*_{5/2}$	6.8	.11
$2f_{5/2}$	$2d^*_{3/2}$	7.4	.11

Table 2 - ph-configurations participating in the twist motion.

Remembering that the position of the twist is insensitive to the residual interaction, the fact that most single particle energies are measured ones contributes strongly to the significance of the results presented. Obviously the concentration of the ph energies around 7 MeV reflects the fluid dynamical findings that the position of the twist is governed by the kinetic energy alone.

In contrast to the twist the spin flip mode does not weigh the high angular momentum ph-amplitudes because one looses one power of ℓ by replacing ℓ_z in (3.5) by the spin operator σ_z. Therefore the spin flip is dispersed over all (in our basis 86) ph states.

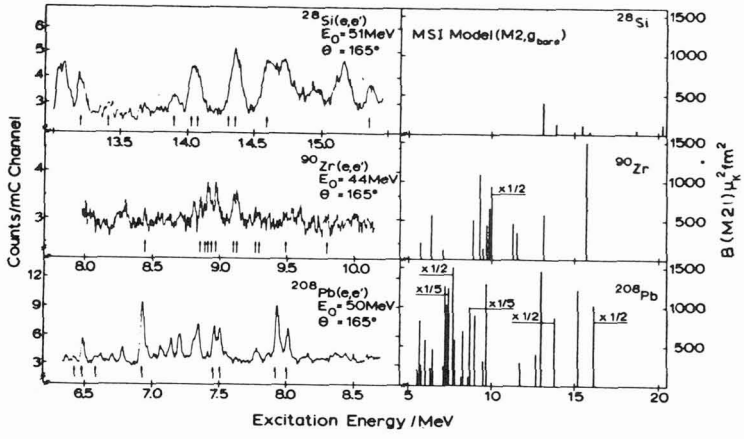

Fig. 12 - (e,e') spectrum of the Darmstandt group /20/. The arrows indicate the position of M2-states.

Fig. 12 shows the (e,e') spectrum from the Darmstadt Linac group /20/ where arrows indicate the position of M2 states. According to the arguments presented the two prominent peaks at 6.9 MeV and at 7.9 MeV must contain predominantly twist strength. Probably accidentally these two peaks agree perfectly with the two twist peaks calculated.

Gamow-Teller resonances

The dispersion of $\vec{\sigma\tau}$ strength due to multipair excitations is of special relevance for the quantitative understanding of isobar-hole admixtures to Gamow-Teller (GT) transitions. It has been suggested /18/ that the giant GT-resonances have long tails due to coupling to 2p-2h states. We have analyzed the $\sigma\tau_-$ -strength functions within our model in both ^{90}Zr and ^{208}Pb. The single particle transitions in the independent particle model are indicated in Fig. 13.

The weaker 3p→3p and 2f→2f transitions in ^{208}Pb are not listed in the figure for simplicity. The antisymmetrized residual interaction V (Table 1) which has been fitted to natural parity excitations is too weak in the spin-isospin channel to reproduce the features of the experimental (p,n) spectra /21/. We therefore readjusted V_{11} (eq. (1.7)) to obtain the proper resonance positions on the 1p-1h level (contributions of order V^2 to the excitation energy are very small). We obtained V_{11} = 228 MeV fm^3 close to the value quoted by Gaarde et al. /22/. After coupling to 2p-2h excitations the $\sigma\tau_-$-distributions displayed in Fig. 14 were obtained. In both

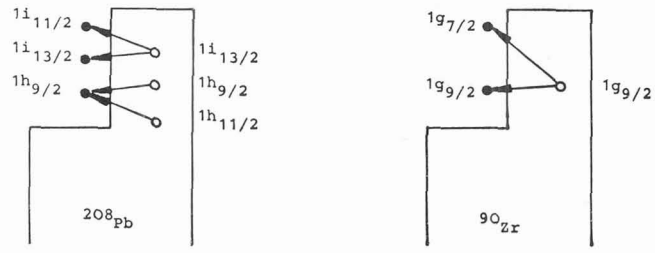

Fig. 13 - Dominant 1p-1h transitions in ^{90}Zr (right part) and ^{208}Pb (left part) including 2p-2h mixing.

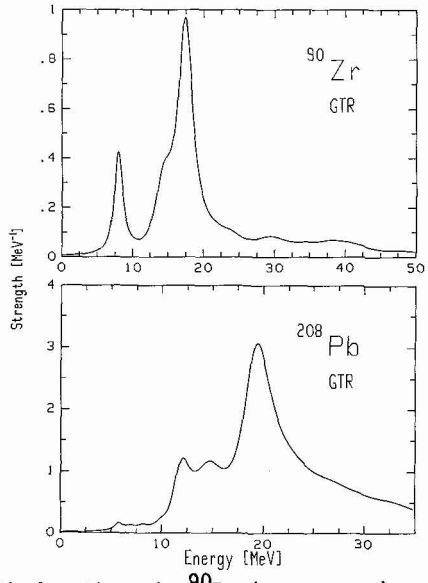

Fig. 14 - GT-strength functions in ^{90}Zr (upper part) and ^{208}Pb (lower part) including 2p-2h mixing.

nuclei the resonances are substantially broadened compared to the 1p1h-distributions and they exhibit long tails on the high energy side. The integrated tail strengths ($\omega > 22.5$ MeV in ^{90}Zr and $\omega > 25$ MeV in ^{208}Pb) are 25 % and 28 % respectively. Since our model is an extended TDA and Pauli unblocking of strength due to ground state correlations is not included we conserve the 3(N-Z) Ikeda sum rule /23/ ($S_{\beta+} = 0$).

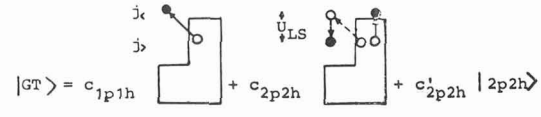

Fig. 15 - Structure of the GT wave function in the vicinity of the resonance peak.

The high-lying GT-peak in ^{90}Zr is mainly built on the $j_> \rightarrow j_<$ transition, in this case $n1g_{9/2} \rightarrow p1g_{7/2}$. There is one specific 2p-2h transition in which a proton in the $j_<$-shell drops to the $j_>$-shell exciting a neutron 1p-1h transition $j_> \rightarrow j_<$ (Fig. 15). If the one body LS potentials for protons and neutrons are the same, this

configuration is degenerate with the $nj_> \rightarrow pj_<$ transition. The coupling matrix element is also large, since the radial wave functions maintain maximum overlap such that this 2p-2h state becomes the dominant decay channel in the vicinity of the peak. In ^{208}Pb the 1p-1h wave function is somewhat more complicated, however, for the $nli_{13/2} \rightarrow pli_{11/2}$ transition which has the largest amplitude the same arguments hold.

REFERENCES

1. G.F. Bertsch, P.F. Bortignon and R.A. Broglia, Rev. Mod. Phys. 55 (1983) 287.
2. R. de Haro, S. Krewald and J. Speth, Nucl. Phys. A388 (1982) 265.
3. B. Schwesinger and J. Wambach, Phys. Lett. in press and to be published.
4. G. Holzwarth and G. Eckart, Z. Physik A283 (1977) 219.
5. G.F. Bertsch, Phys. Lett. 37B (1971) 470.
6. C.H. Aldrich III, C.J. Pethick and D. Pines, Phys. Rev. Lett. 37 (1977) 845.
7. G.F. Bertsch et al., Phys. Lett. 80B (1979) 161.
8. S.O. Bäckman, O. Sjöberg and A.D. Jackson, Nucl. Phys. A321 (1979) 10.
9. R. Pitthan, in "Giant Multipole Resonances", Proceedings, Oak Ridge, TN, 1979, ed. Fred E. Bertrand (Harwood Academic Publishers, 1980) p. 161.
10. J.D. Bowman, M.B. Johnson and J.W. Negele, Phys. Rev. Lett. 46 (1981) 1614.
11. J.D. Bowman et al., Phys. Rev. Lett. 50 (1983) 1195.
12. N. Auerbach and A. Klein, Nucl. Phys. A395 (1983) 77.
13. W.D. Myers and W.J. Swiatecki, Nucl. Phys. 81 (1966) 1;
    W.D. Myers and W.J. Swiatecki, Ann. Phys. 84 (1974) 186.
14. G.A. Rinker and J. Speth, Nucl. Phys. A306 (1978) 360.
15. G.E. Brown, J.S. Dehesa and J. Speth, Nucl. Phys. A330 (1979) 290.
16. J. Wambach, V.K. Mishra and Li Chu-Hsia, Nucl. Phys. A380 (1982) 285.
17. J. Treiner, these Proceedings.
18. G.F. Bertsch and I. Hamamoto, Phys. Rev. 26C (1982) 1323.
19. G. Kühner et al., Phys. Lett. 104B (1981) 189;
    H.P. Morsch et al., preprint Jülich, 1983.
20. R. Frey et al., Phys. Lett. 74B (1978) 45;
    W. Knüpfer et al., Phys. Lett. 77B (1978) 367.
21. C.D. Goodman, Nucl. Phys. A374 (1982) 241.
22. C. Gaarde et al., Nucl. Phys. A369 (1981) 258.
23. K.I. Ikeda, S. Fujii and J.I. Fujita, Phys. Lett. 3 (1963) 271.